Bumpless Automatic Transfer for a Switched-Doubly-Fed-Machine Propulsion Drive

Arijit Banerjee, *Student Member, IEEE*, Arthur H. Chang, *Student Member, IEEE*, Kawin North Surakitbovorn, Steven B. Leeb, *Fellow, IEEE*, and James L. Kirtley, Jr., *Life Fellow, IEEE*

***Abstract*—Variable-speed drives (VSDs) combined with doubly-fed machines (DFMs) offer interesting flexibility for power electronic drive design. These also provide opportunities for controlling interactions with an ac grid. Design options are most versatile for the VSD DFM when the machine stator can be operated from an ac or a dc source, selected as appropriate. This paper presents a silicon-controlled rectifier (SCR)-based transfer switch that can connect the stator of the DFM either to an ac source or a dc source "on-the-fly." Current commutations of the SCRs and a "bumpless" transition in shaft behavior are both controlled from the rotor. Experimental results demonstrate wide-speed-range and four-quadrant operation of the drive achieved with a rotor converter rating that is one third of the DFM power rating.**

***Index Terms*—Commutation, control, doubly-fed machine (DFM), power electronic converter, SCR, static transfer switch (STS).**

I. Introduction

VARIABLE-SPEED drives (VSDs) are critical in many industrial and commercial applications. These drives are increasingly relevant not only for process and motion control but also for optimizing energy consumption, e.g., in heating, ventilation, and air-conditioning units. The demand for efficient, cost-effective, and sustainable solutions for different industrial sectors has led to a larger market penetration of high-power VSDs [1]. Essentially all machine types have been explored for high-power VSDs, including squirrel-cage induction [2], synchronous [3], permanent magnet [4], doubly-fed induction [5], and superconducting machine [6]. At higher voltage and current levels (e.g., for machines in the megawatt range and beyond), creating a VSD using a power converter becomes a challenge. VSD power converters at higher power levels might require combining multiple semiconductor devices in series and parallel, due to limited available device ratings [7]. Operating switching frequencies become constrained to limit the switching losses in the devices leading to poorer dynamic performance and greater harmonic distortion of the motor and the line-side waveforms of the drive [8].

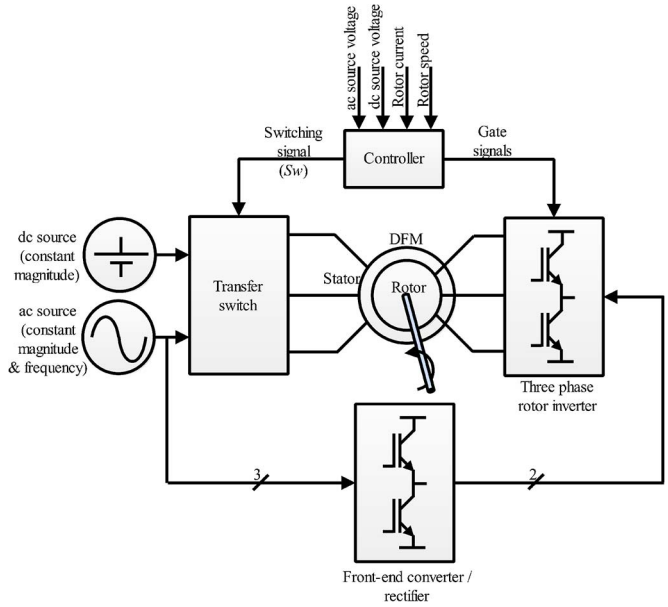

Fig. 1. Proposed configuration of the switched-DFM drive.

A doubly-fed machine (DFM) offers useful possibilities for reducing the required rating of the associated power converter. This has made the DFM attractive, for example, in wind generation applications where a limited range of operating speed around synchronous speed substantially reduces the required power converter size, typically to one third compared with that of the electrical machine size [9]. This size reduction is lost if the required operating speed range of the drive is increased.

In applications where a dc source is available, or can be made from an existing ac source (as in a ship propulsion drive), a switched-DFM drive can enable wide-speed-range operation with reduced power converter rating [10]. The drive operates in one of the two modes as shown in Fig. 1.

- DC mode: At low speeds, the stator of the DFM is connected to the dc source, making the DFM behave as a wound-field synchronous machine.
- AC mode: At higher speeds, the stator is switched to the fixed-frequency ac supply, transforming the DFM to the traditional doubly-fed induction machine.

The rotor of the DFM is always fed from a controlled converter. The rotor converter rating can be a third of the machine power

Manuscript received September 25, 2014; revised December 5, 2014; accepted January 9, 2015. Date of publication February 20, 2015; date of current version July 15, 2015. Paper 2014-IDC-0649.R1, presented at the 2014 IEEE Applied Power Electronics Conference and Exposition, Fort Worth, TX, USA, March 16–20, and approved for publication in the IEEE Transactions on Industry Applications by the Industrial Drives Committee of the IEEE Industry Applications Society. This work was supported in part by the MIT-Skoltech SDP Program, in part by The Grainger Foundation, and in part by the MIT EECS SuperUROP Program.

The authors are with the Department of Electrical Engineering and Computer Science, Massachusetts Institute of Technology, Cambridge, MA 02139 USA (e-mail: arijit@mit.edu; arthurhc@mit.edu; north@stanford.edu; sbleeb@mit.edu; kirtley@mit.edu).

Color versions of one or more of the figures in this paper are available online at http://ieeexplore.ieee.org.

Digital Object Identifier 10.1109/TIA.2015.2404914

rating while operating on a speed range of −0.5 to 1.5 p.u. (normalized to synchronous speed corresponding to the ac source frequency). Furthermore, the operating speed range of the drive can be extended to ±1.5 p.u. with the same rotor converter power rating by changing the phase sequence of the ac source connection to the stator. A reduction in the required converter rating translates into savings on the transformer and filter size for the overall drive [10]. The proposed drive can be seamlessly controlled across the complete operating speed range [11].

A critical challenge for practically implementing a switched-DFM drive is developing a cost-effective switching circuit that can connect the stator to either of the sources, dc or ac, on-the-fly and reversibly. A complex switching circuit in the DFM stator made with self-commutating devices such as integrated gate-commutated thyristor, gate turn-off thyristor, and insulated-gate bipolar transistor [12] is counter to the benefit of a reduced rotor converter. Alternatively, sluggish mechanical switches [13] controlling the stator connection can significantly impact the shaft behavior during transition, leading to poorly controlled speed/torque variations [14], and even forcing the switched-DFM drive to operate in two isolated stages—starting and operating [15]. Using SCRs for the stator transition between ac and dc voltages can provide a balance between complexity and performance. SCRs are still some of the most capable high-power devices available [16]. A single device can handle large currents and block large voltages. However, SCRs require special considerations to ensure device turn-off.

This paper presents an SCR-based static transfer switch (STS) that can connect the stator of the proposed DFM drive to either the ac or the dc source "on-the-fly," with well-controlled speed/torque variations at the shaft output. Two sets of SCRs are used to connect the sources to the stator of the DFM. Only one set is turned on during each operating mode of the DFM drive to connect the corresponding source to the stator. The dc-side SCRs are continuously on when the DFM drive is operating in the dc mode. The ac-side SCRs switch at line frequency in the ac mode of operation of the DFM drive. This minimizes switching losses in the overall transfer switch without increasing harmonic distortions of the stator waveform.

Development of an STS suitable for the proposed DFM drive is focused on two different aspects. Appropriate conditions based on the DFM stator current and the dc and ac source voltages are derived, which ensure natural commutation of all outgoing SCRs simultaneously during both the dc-to-ac and ac-to-dc transitions. Next, these conditions are superimposed with requirements from the DFM perspective, which can ensure bumpless mechanical behavior at the shaft. During mode transitions, careful control of the rotor power electronics not only ensures natural commutation of the outgoing SCR bank but also makes a seamless transition at the shaft.

II. STS Analysis

SCR-based STSs have been extensively used to supply uninterrupted power to critical loads [17]–[21]. A traditional operational scheme in these STS is detecting a disturbance in the primary ac source, followed by transitioning of the load to an alternate ac source, both of the sources being of identical voltage and frequency. However, for the proposed DFM drive, the transfer occurs between an ac and a dc source of widely different voltage magnitudes, with the load having variable power factor and regeneration capability. This is a challenge because the two sources cannot be "synchronized" [22] for transfer. Additionally, the load, in this case, the DFM, cannot withstand partial phase transfer [23]. The transfer operation between the dc and ac source is triggered based on the operating speed of the DFM and the designed mode-transition speed. This makes the source-transfer mechanism integral to the switched-DFM drive operation rather than as a means to provide occasional back-up power.

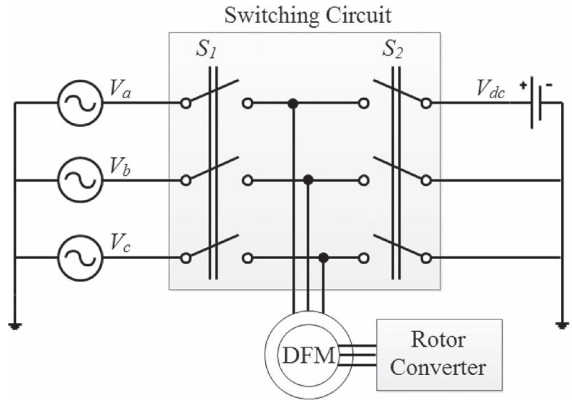

Fig. 2. Ideal transfer switch connected to the DFM stator winding to alter the connection between ac and dc sources as necessary, based on operating speed.

This section begins with a review of the ideal requirements for a transfer of the stator of the DFM between an ac and a dc source. Conditions are identified in an ac cycle such that all three phases can undergo simultaneous natural commutation during the source transition.

A. Requirements for an Ideal Transfer Switch

A schematic of an ideal transfer switch connected to the DFM is shown in Fig. 2. The DFM can be connected to either of the two sources, i.e., ac or dc, based on the configuration of switch S_1 and S_2. It is assumed that the dc and the ac sources share a common reference. In practice, the dc source may be created from the ac source using a transformer rectifier. In dc mode, the dc source only supplies the resistive losses in the stator of the DFM. Consequently, the power rating of the transformer rectifier is a fraction of the DFM power rating.

Several characteristics of transfer-switch operation are required.

- The ac and dc sources should not be shorted, i.e., S_1 and S_2 cannot be *ON* simultaneously.
- The DFM stator current should not be instantaneously interrupted, i.e., S_1 and S_2 cannot be both *OFF* abruptly with a nonzero DFM stator current.
- The three phases should always switch together, i.e., the three phases of the stator are connected to a single source, either dc or ac, at any instant. This ensures that the DFM will not experience severely unbalanced stator voltages that can lead to unacceptable disturbances in the stator flux.

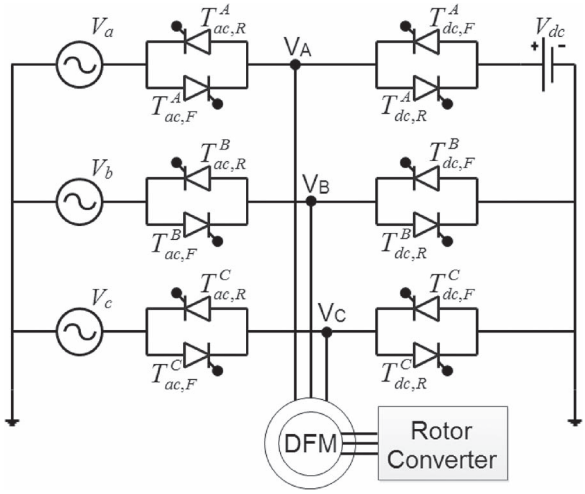

Fig. 3. Three-phase SCR-based transfer switch connected to the stator of the DFM.

A few other characteristics are also necessary.

- The DFM should experience minimal perturbation in electromagnetic torque and speed at the shaft during source transition.
- Additional "supporting" circuitry, e.g., forced commutation circuit, should be minimized to limit cost and complexity.

Because switch S_1 should block bidirectional voltage and carry bidirectional current, an antiparallel configuration of SCRs for each phase is required as in a standard STS. Switch S_2 appears to carry only unidirectional current and to block bidirectional voltage, such that a single SCR for each phase is sufficient. However, the DFM stator-current polarity can reverse during load transients in the dc mode and during the ac-to-dc source transition. Therefore, an antiparallel configuration of the SCRs for each phase is required to replace the ideal switch S_2.

B. Identification of Instances for Natural Commutation for a Three-Phase SCR-Based Transfer Switch

The proposed SCR-based three-phase transfer switch connected to the stator of the DFM is shown in Fig. 3. One of the sources is dc of magnitude $V_{\rm dc}$, and the other is a three-phase ac source represented by phase voltages V_a, V_b, and V_c. The rotor is fed from the controlled converter.

1) Transition From DC to AC Source: Assuming initially that the stator of the DFM is connected to the dc source, at steady state, the stator current is positive in the A phase and negative in the B and C phases. This implies that SCRs $T^A_{{\rm dc},F}$, $T^B_{{\rm dc},R}$, and $T^C_{{\rm dc},R}$ are conducting. These three SCRs are classified as the "conducting bank." The complementary SCRs $T^A_{{\rm dc},R}$, $T^B_{{\rm dc},F}$, and $T^C_{{\rm dc},F}$, classified as the "nonconducting bank," do not take part during this transition, and the gate signals to these SCRs are disabled at the onset of the transition. A commutation diagram can be established for all three phases using the stator A-phase winding axis as reference, as shown in Fig. 4. The dc-source voltage magnitude, shown as a dashed line, is relatively small compared with the ac-source voltage. Before the transition, the stator voltage vector $\overline{V_{\rm dc}}$ (where $|\overline{V_{\rm dc}}| = (2/3)V_{\rm dc}$) and the current vector $\overline{I_s}$ are both stationary, aligned, and oriented toward the A-phase axis, whereas the incoming ac voltage vector $\overline{V_{\rm ac}}$ is rotating at the ac-source frequency, i.e., $\omega_{\rm ac}$.

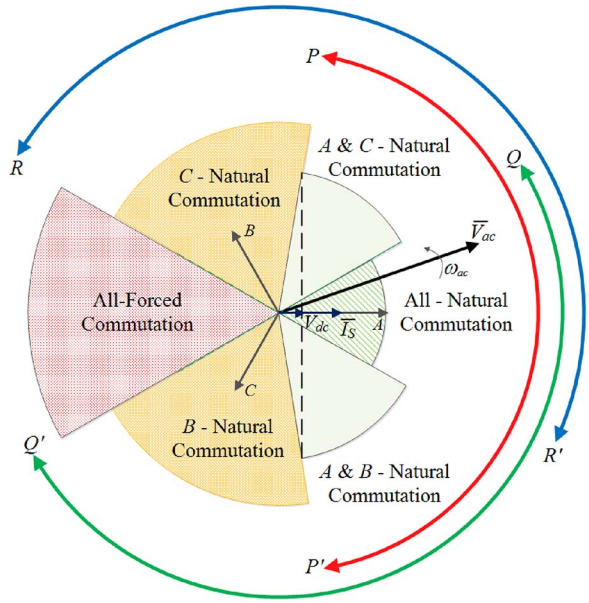

Fig. 4. Commutation diagram during dc-to-ac source transition.

For the A phase, turning off the gate signal to SCR $T^A_{{\rm dc},F}$ and firing SCR $T^A_{{\rm ac},F}$ when the ac-source A-phase voltage is greater than the dc-source voltage naturally steers the stator current from the dc to ac source. This implies that the ac-source voltage vector must be within the arc PP' in Fig. 4 to ensure natural commutation of SCR $T^A_{{\rm dc},F}$. Similarly, for the B and C phases, SCRs $T^B_{{\rm dc},R}$ and $T^C_{{\rm dc},R}$ can be turned off naturally by deactivating the gate signal to these SCRs and firing gate pulses to SCRs $T^B_{{\rm ac},R}$ and $T^C_{{\rm ac},R}$ during the negative half cycle of the B and C phase ac-source voltages, respectively. These conditions are met when the ac-source voltage vector is within the arc QQ' and RR', respectively, in the commutation diagram in Fig. 4. Different sectors evolve in the commutation diagram, which demarcates possible commutation for the outgoing three-phase SCRs. The sector of $\pm 30^\circ$ where all the three arcs overlap indicates the special region for the ac-source voltage vector where natural commutation can occur for the dc-side conducting bank.

After the source transition, SCRs $T^A_{{\rm ac},F}$, $T^B_{{\rm ac},R}$, and $T^C_{{\rm ac},R}$ continue to supply the DFM stator current. These SCRs form the "succeeding bank." With a sufficient dead time, depending on the turn-off time of the SCRs, the gate signals to the remaining SCRs on the ac side $T^A_{{\rm ac},R}$, $T^B_{{\rm ac},F}$, and $T^C_{{\rm ac},F}$, collectively named as the "concluding bank," are enabled. This completes the transfer of the stator of the DFM to the ac source.

2) Transition From AC to DC Source: Conversely, when the stator of the DFM is initially connected to the ac source, all ac-side SCRs $T^A_{{\rm ac},F}$, $T^A_{{\rm ac},R}$, $T^B_{{\rm ac},F}$, $T^B_{{\rm ac},R}$, $T^C_{{\rm ac},F}$, and $T^C_{{\rm ac},R}$ operate on 180° conduction mode depending on the stator voltage and current. This implies that three of the six SCRs conduct at the instant of transition, which constitutes the conducting bank. The remaining three complementary SCRs, forming the nonconducting bank, do not influence the transition, and the gate

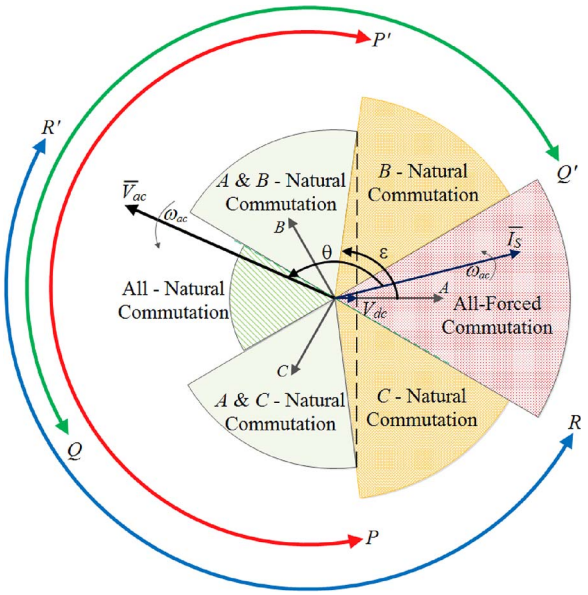

Fig. 5. Commutation diagram during ac-to-dc source transition.

signals to this bank can be turned off. On the dc side, three SCRs (succeeding bank) turn on at the instant of transition for each phase, commutating the current from the ac source to the dc source. The remaining three dc-side SCRs (concluding bank) are turned on after a sufficient dead time to avoid shoot-through problems between the ac and dc sources. Unlike in the dc-to-ac source transition, the SCRs that constitute these four banks depend on the stator-current polarity at the instant of transition. Consequently, the conditions of the source voltages required for natural commutation of the conducting bank during the ac-to-dc source transition need to be determined based on the stator-current polarity.

For example, when the stator-current vector $\overline{I_s}$ is in the sector of $\pm 30^\circ$ in Fig. 5, SCRs $T^A_{\mathrm{ac},F}$, $T^B_{\mathrm{ac},R}$, and $T^C_{\mathrm{ac},R}$ constitute the conducting bank, whereas SCRs $T^A_{\mathrm{ac},R}$, $T^B_{\mathrm{ac},F}$, and $T^C_{\mathrm{ac},F}$ form the nonconducting bank. During the period when the ac source A-phase voltage is less than the dc source voltage, turning off the gate signal to SCR $T^A_{\mathrm{ac},F}$ and firing SCR $T^A_{\mathrm{dc},F}$ will naturally commutate the stator A-phase current from the ac source to the dc source. This condition is met when the ac-source voltage vector is within the arc PP'. Similarly, for the B and C phases, SCRs $T^B_{\mathrm{ac},R}$ and $T^C_{\mathrm{ac},R}$ can naturally commutate the stator current to SCRs $T^B_{\mathrm{dc},R}$ and $T^C_{\mathrm{dc},R}$ at the instant when the ac source B and C phase voltages are positive, shown by arcs QQ' and RR', respectively. In this case, SCRs $T^A_{\mathrm{dc},F}$, $T^B_{\mathrm{dc},R}$, and $T^C_{\mathrm{dc},R}$ form the succeeding bank. To ensure all the three phases undergo natural commutation at the same instant, the ac-source voltage vector must be within 150° and 210° where the arc PP', QQ', and RR' overlap, as shown in Fig. 5. Finally, the complementary dc-side SCRs $T^A_{\mathrm{dc},F}$, $T^B_{\mathrm{dc},R}$, and $T^C_{\mathrm{dc},R}$ in the concluding bank are provided with gate pulses after a sufficient dead time to complete the source transition.

This analysis can be extended for other possible polarities of the three-phase stator current such that natural commutation of the outgoing ac-side SCRs is ensured. The sectors of natural and forced commutation for each phase also rotate along with the stator-current vector location. Table I summarizes the SCRs that form the conducting and succeeding banks at the instant of transition depending on the stator-current polarity. Moreover, this table highlights the requirement on the ac-source voltage vector to make simultaneous natural commutation of the conduction bank SCRs. The angle ε in Table I depends upon the magnitudes of the dc- and the ac-source voltage vector and can be calculated as

$$\varepsilon = \cos^{-1}\frac{|\overline{V_{\mathrm{dc}}}|}{|\overline{V_{\mathrm{ac}}}|}. \tag{1}$$

Based on Table I, the common requirement for simultaneous natural commutation of the ac-side SCRs is that the stator power factor angle θ must be between 120° and 240° irrespective of the location of the stator current vector. The complementary region of natural commutation of the conduction bank SCRs between the two mode transitions, i.e., dc-to-ac in Fig. 4 and ac-to-dc in Fig. 5, is due to the relative magnitude of the source voltages, as expected.

III. Control of DFM Drive With Transfer Switch

The three-phase SCR switch analysis using the commutation diagrams shown in Figs. 4 and 5 indicates that transitions between the dc- and ac-mode operation of the DFM can occur on-the-fly without shorting the sources or interrupting the load current. With appropriate constraints on the ac-source voltages depending on the DFM stator current at the instant of transition, a simultaneous natural commutation for all the outgoing SCRs can be ensured. These constraints for natural commutation must be observed to avoid the need for additional commutation circuitry.

However, ensuring a smooth and controlled speed/torque production and a mechanically bumpless shaft behavior during the transition is also essential. Here, the DFM constraints are determined. Furthermore, the appropriate rotor converter control is described for making the transition as smooth as possible while crossing between the low- and high-speed operating regions. The effect of the demanded drive torque on the operation of the SCR-based transfer switch is examined. As a precursor, this section revisits ideal mode transition conditions to ensure a mechanically bumpless transition from the DFM perspective using a synchronizer. Reference [11] presents more detailed analysis and functionality of the synchronizer.

A. Synchronizer

The DFM is connected to the ac source when the rotor speed is greater than the designed transition speed. Conversely, it is connected to the dc source in low-speed mode. A mode transition is required as the speed crosses the operating boundary in either direction. This transition must occur at a proper instant when the "incoming" source voltage is as consistent as possible with the operating state of the DFM prior to transition to minimize disturbances in the stator flux and in the electromagnetic torque. The synchronizer module measures the incoming source voltage vector, transforms the measurement to the stator-flux reference frame, and waits for the proper match of the d-axis

TABLE I
CLASSIFICATION OF OUTGOING AC-SIDE AND INCOMING DC-SIDE SCRS FOR AN AC-TO-DC SOURCE TRANSITION BASED ON THE STATOR-CURRENT VECTOR LOCATION

Location of stator current vector	Conducting bank (ac side)	Succeeding bank (dc side)	Required ac source voltage vector
$-30^\circ < \angle\overline{I_s} < 30^\circ$	$T^A_{ac,F}, T^B_{ac,R}, T^C_{ac,R}$	$T^A_{dc,F}, T^B_{dc,R}, T^C_{dc,R}$	$150^\circ < \angle\overline{V_{ac}} < 210^\circ$
$30^\circ < \angle\overline{I_s} < 90^\circ$	$T^A_{ac,F}, T^B_{ac,F}, T^C_{ac,R}$	$T^A_{dc,F}, T^B_{dc,F}, T^C_{dc,R}$	$210^\circ < \angle\overline{V_{ac}} < 360^\circ - \varepsilon$
$90^\circ < \angle\overline{I_s} < 150^\circ$	$T^A_{ac,R}, T^B_{ac,F}, T^C_{ac,R}$	$T^A_{dc,R}, T^B_{dc,F}, T^C_{dc,R}$	$360^\circ - \varepsilon < \angle\overline{V_{ac}} < 330^\circ$
$150^\circ < \angle\overline{I_s} < 210^\circ$	$T^A_{ac,R}, T^B_{ac,F}, T^C_{ac,F}$	$T^A_{dc,R}, T^B_{dc,F}, T^C_{dc,F}$	$-30^\circ < \angle\overline{V_{ac}} < 30^\circ$
$210^\circ < \angle\overline{I_s} < 270^\circ$	$T^A_{ac,R}, T^B_{ac,R}, T^C_{ac,F}$	$T^A_{dc,R}, T^B_{dc,R}, T^C_{dc,F}$	$30^\circ < \angle\overline{V_{ac}} < \varepsilon$
$270^\circ < \angle\overline{I_s} < 330^\circ$	$T^A_{ac,F}, T^B_{ac,R}, T^C_{ac,F}$	$T^A_{dc,F}, T^B_{dc,R}, T^C_{dc,F}$	$\varepsilon < \angle\overline{V_{ac}} < 150^\circ$

TABLE II
MACHINE PARAMETERS

DFM Parameters	
Stator resistance (R_s)	$3.575\ \Omega$
Rotor resistance (R_r)	$4.229\ \Omega$
Stator leakage inductance (L_{ls})	$9.6\ mH$
Rotor leakage inductance (L_{lr})	$9.6\ mH$
Mutual inductance (M)	$165\ mH$
Moment of inertia (J)	$0.01\ kgm^2$
Frictional coefficient (B)	$0.0025\ Nm - s/rad$
PMSG Parameters	
Back emf constant	$0.1061\ V - s/rad$
Stator resistance	$0.5\ \Omega$

and the q-axis (leads d-axis by 90° by convention) components to initiate the transition using Sw signal in Fig. 1.

For dc-to-ac mode transition, the d-axis component of the incoming ac voltage is matched to the existing d-axis voltage from the dc-source connection, which minimizes flux-magnitude perturbation. The synchronizer chooses a transition time when the incoming ac voltage appears with a positive q-axis component, permitting the stator-flux frequency to transition from zero to a positive finite value. The required conditions become apparent from examining the DFM machine equations as shown in [11].

In the case of ac-to-dc mode transition, the d-axis component of the incoming dc voltage is matched to the existing d-axis voltage from the ac-source connection. A negative q-axis component of the incoming dc voltage ensures proper transition of stator-flux frequency to zero. Adhering to the requirement for the ac-to-dc transition is considerably relaxed compared with the dc-to-ac transition due to the presence of a stator-flux controller on the DFM rotor-side control that can affect the stator-flux magnitude in the dc mode. Analysis using a simplified nonlinear DFM plant model shows that the ac-to-dc transition can be performed over a wider region in the ac cycle without degrading the drive performance.

Satisfying the synchronizer constraint and the natural commutation region constraint of the outgoing SCRs will ensure the least perturbation on the DFM without requiring forced commutation circuits for the SCRs. For the mode transitions, the demanded drive torque at the transition instant is critical in determining whether the two constraints can be simultaneously satisfied.

B. DC-to-AC Mode Transition With DFM Constraints

In the low-speed dc mode, the rotor d-axis current controls the stator-flux magnitude while the rotor q-axis current sets the electromagnetic torque. The electromagnetic torque is

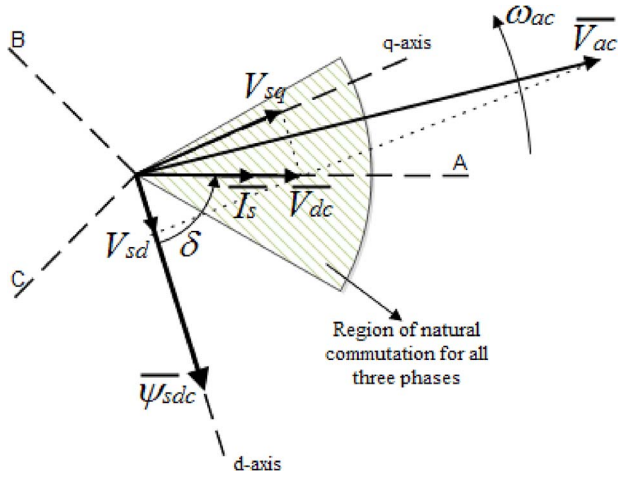

Fig. 6. Space vector diagram during dc-to-ac transition that ensures minimum flux perturbation and natural commutation of the conducting SCR bank under high-drive-torque demand.

determined by the stator-flux magnitude and the rotor q-axis current, i.e.,

$$\tau_{\rm dc} = -\frac{3}{2}\frac{P}{2}\frac{M}{L_s}|\overline{\psi_{sdc}}|I_{rq}. \tag{2}$$

The rotor q-axis current can be expressed in terms of the stator q-axis current and the machine parameters (see Table II), yielding a torque expression

$$\tau_{\rm dc} = \frac{3}{2}\frac{P}{2}|\overline{\psi_{sdc}}|I_{sq}. \tag{3}$$

Fig. 6 shows the stator voltage vector $\overline{V_{\rm dc}}$, stator current vector $\overline{I_s}$, and the stator-flux vector $\overline{\psi_{sdc}}$, all of which are stationary relative to the DFM stator axis in the low-speed dc mode. Designating the angle between the stator-flux vector and the stator voltage vector as δ, (3) is represented as

$$\tau_{\rm dc} = \frac{3}{2}\frac{P}{2}|\overline{\psi_{sdc}}||\overline{I_s}|\sin\delta. \tag{4}$$

If the drive-torque demand is sufficiently large, (4) indicates that the angle δ is large as depicted in Fig. 6. Under this condition, for a transition to ac mode, the synchronizer chooses an instant when the "incoming" ac voltage vector $\overline{V_{\rm ac}}$ exhibits a d-axis component that matches the existing d-axis stator voltage. This precise instant is illustrated in Fig. 6. As $\overline{V_{\rm ac}}$ is within the sector of natural commutation for all three phases (as derived in Section II-B), a dc-to-ac mode transition is ensured with the least perturbation to the DFM. All of the dc-side conducting banks undergo natural commutation.

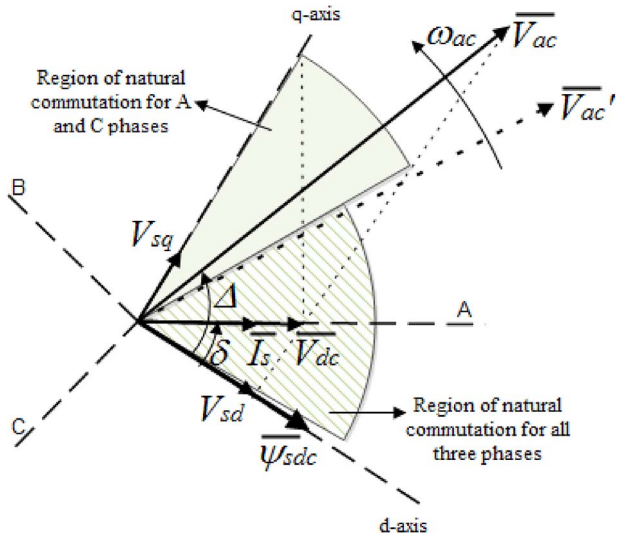

Fig. 7. Space vector diagram during dc-to-ac transition that ensures minimum flux perturbation and natural commutation of conducting SCR bank under low-drive-torque demand.

However, under low-drive-torque demand, natural commutation in all the three phases might not occur. This situation is illustrated in Fig. 7. In a case with the angle δ relatively small, the synchronizer does not find an instant within the arc of natural commutation that also matches the d-axis component of the "incoming" ac-source voltage to that of the existing d-axis component of the stator voltage.

Fortunately, for transition instances with low-drive-torque demand, the rotor power electronics are lightly loaded and have plenty of capability to modulate the d-axis rotor current to damp the stator-flux transient. Hence, in lightly load conditions, the synchronizer chooses the best or "last possible" instant to make the transition, at $\overline{V_{\rm ac}}'$ in Fig. 7. This moment is when natural commutation for all outgoing dc-side SCRs is still possible. The occurrence of larger swings of stator-flux transient is damped by a full-state feedback controller that minimizes the stator-flux oscillation [11].

The boundary that defines a low-drive-torque demand is determined by the selected operating stator-flux magnitude in the dc mode and the dc- and ac-source voltages. The boundary condition of low-drive-torque demand occurs when the synchronizer finds $\overline{V_{\rm ac}}$ exactly on the edge of the sector of natural commutation for all the three phases at the instant when the d-axis component of the source voltages match, i.e., from the geometry shown in Fig. 7, i.e.,

$$V_{sd} = |\overline{V_{\rm dc}}| \cos \delta_{\rm min} = |\overline{V_{\rm ac}}| \cos \Delta \tag{5}$$

and

$$\Delta - \delta_{\rm min} = \frac{\pi}{6}. \tag{6}$$

Solving (5) and (6), the boundary of "low drive torque" is given by $\delta_{\rm min}$, i.e.,

$$\delta_{\rm min} = \tan^{-1}\left(\sqrt{3} - 2\frac{|\overline{V_{\rm dc}}|}{|\overline{V_{\rm ac}}|}\right). \tag{7}$$

The minimum torque below which the demanded drive torque is termed "low" can be written using (4) and (7) as

$$\tau_{\rm dc,min} = \frac{3}{2}\frac{P}{2}|\overline{\psi_{sdc}}|\frac{|\overline{V_{\rm dc}}|}{R_s}\sin\left[\tan^{-1}\left(\sqrt{3} - 2\frac{|\overline{V_{\rm dc}}|}{|\overline{V_{\rm ac}}|}\right)\right]. \tag{8}$$

C. AC-to-DC Mode Transition With DFM Constraints

The two major differences in the high-speed ac mode of DFM operation compared with that of dc-mode operation are, first, the angle between the stator voltage and the stator flux (δ) is relatively fixed and is close to 90° independent of the mechanical load (assuming small stator resistance) and, second, the stator voltage $\overline{V_{\rm ac}}$, the stator current $\overline{I_s}$, and the stator flux $\overline{\psi}_{sac}$ vectors rotate at the ac-source frequency relative to the stationary dc-source voltage vector $\overline{V_{\rm dc}}$ and the stator-winding axis. The stator voltage and current must be at least 120° out of phase for the ac-to-dc transition to occur with all outgoing ac-side SCRs undergoing natural commutation simultaneously as shown in Section II-B. This implies that the active power flowing to the stator must be negative during the transition, which is inherently achieved by the drive operation. The mode transition of ac to dc is necessary when the drive speed goes below the designed transition speed, which requires a braking action and, therefore, a reverse power flow in the stator. The braking torque is commanded using the rotor q-axis current. The remaining requirement on maintaining the stator power factor can be achieved using the reactive power controller on the rotor power electronics. The reactive-power controller commands the rotor d-axis current to create the required phase between the stator voltage and the current for natural commutation of the outgoing ac-side SCRs (conducting bank).

With properly controlled rotor currents, the ac-to-dc source transition can be initiated during any part of the ac cycle based on the values in Table I. This flexibility is due to the presence of an antiparallel SCR bank on the dc side that can potentially shorten the ac-to-dc source transition time. However, a careful choice of transition instant is necessary to ensure smooth transition of the stator flux (from ac to dc) of the DFM and, therefore, a controlled torque output at the shaft. To illustrate the correct transition region for ac-to-dc transition from a DFM perspective, the state-plane analysis is used, as in [11]. Assuming a large rotor-current controller bandwidth, the nonlinear DFM plant during source transition can be simplified in state-space form as

$$\frac{d}{dt}\begin{bmatrix}\psi_s \\ \delta\end{bmatrix} = \begin{bmatrix}-\frac{R_s}{L_s}\psi_s + V_{\rm dc}\cos\delta \\ -\frac{V_{\rm dc}\sin\delta}{\psi_s} + \frac{1}{\psi_s^2}\frac{4R_s}{3P}\tau\end{bmatrix} + \begin{bmatrix}\frac{MR_s}{L_s} \\ 0\end{bmatrix} I_{rd}. \tag{9}$$

This is identical to the plant model derived in [11] except that (9) represents the DFM after the transition of the stator to the dc source. The initial condition of the stator-flux magnitude ψ_s is equal to the ac-mode stator-flux magnitude $|\overline{\psi_{sac}}|$ prior to the transition. Similarly, the initial condition for the angle δ is determined by the switching instant from the ac source to the dc source. After the transition to the dc source, the rotor d-axis current is commanded based on the stator-flux

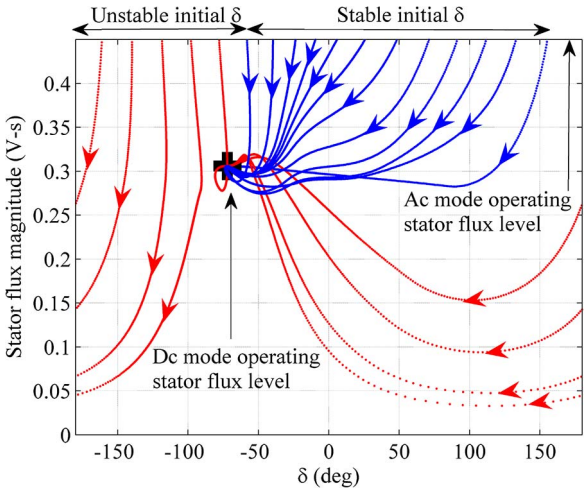

Fig. 8. Phase plane analysis: Determination of the desired switching instant during the ac-to-dc transition. Improper switching instant can lead to a collapse of the stator-flux magnitude, leading to an uncontrolled shaft torque perturbation.

controller with an output limiter that follows a control law given by

$$I_{rd}^{*}=\left(K_p+\frac{K_i}{s}\right)\left[|\overline{\psi_{sdc}}|-\psi_s\right]-\frac{L_s}{MR_s}V_{\rm dc}\cos\delta;\quad |I_{rd}^{*}|<I_{rd,\rm limit}. \tag{10}$$

The assumption of large rotor-current controller bandwidth allows to couple (9) and (10) by

$$I_{rd}=I_{rd}^{*}\in[-I_{rd,\rm limit},I_{rd,\rm limit}]. \tag{11}$$

The nonlinear dynamics for the state trajectories are shown in Fig. 8. It is assumed that the initial ac-mode stator-flux magnitude is 0.45 V-s, whereas the final dc-mode stator-flux magnitude is 0.3 V-s (based on the prototype DFM drive design). Based on the instant of transition, governed by the initial δ, the states for the nonlinear system described by (9), (10), and (11) follow different trajectories during the ac-to-dc mode transition. The steady-state condition for angle δ is determined by the demanded braking torque as given by (4). As can be seen in Fig. 8, the least perturbation in the stator flux during the transition occurs when the initial δ is within the stable zone marked in Fig. 8. For other switching instances, the stator-flux magnitude completely collapses, leading to a significant uncontrolled shaft torque behavior. Therefore, for a guaranteed stable ac-to-dc transition, the desirable range of the stator-flux angle at the instant of transition must be within zero and 90°. With the stator flux lagging the stator voltage nearly by 90°, the corresponding suitable region is when the ac-source voltage vector is within 0° and 90° with respect to the stator A-phase axis.

The requirement of reverse active-power flow necessary for the natural commutation of the ac-side SCRs might not be satisfied under certain drive-torque requirements. For example, a gradual ramp-down command for the drive reference speed, or a mode transition initiated because of load disturbances does not necessarily need a negative drive torque at the transition speed. In these cases, either a forced commutation circuit should be added on to the ac-side SCRs, or a secondary transition speed

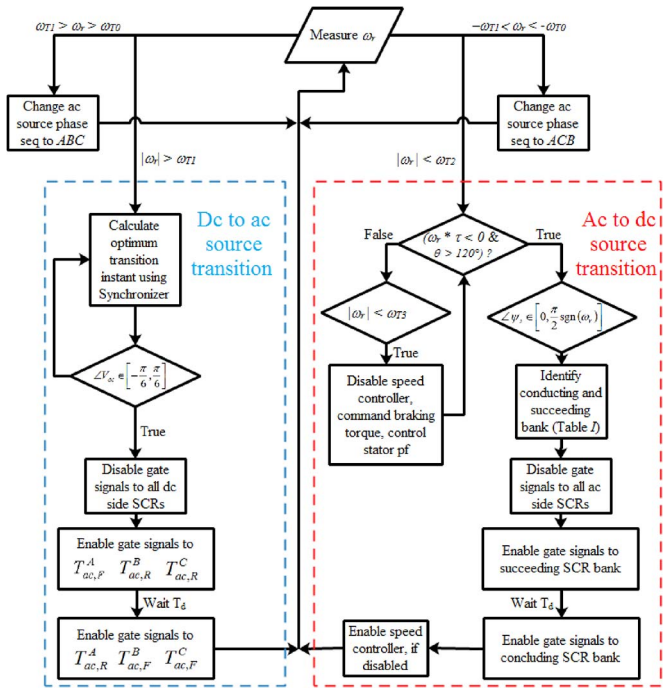

Fig. 9. Flowchart for controlling the SCR-based transfer switch and the ac-source, phase-sequence, change-over relay for four-quadrant operation of a switched-DFM drive.

can be designed depending on the applications. If the rotor speed goes below the designed secondary transition speed, the speed controller is momentarily disabled with deliberate sufficient braking torque commanded to the drive. This ensures proper conditions necessary for the natural commutation of the ac-side conducting bank. The speed controller comes back into the control loop after the mode transition. Fluctuations to drive speed are insignificantly perturbed during this short maneuver because of the presence of the mechanical inertia of the drive.

D. Operation of the Transfer Switch and Phase Change Over Relay

Based on the above analysis, a flowchart of the transfer-switch operation is outlined in Fig. 9. A hysteresis band is introduced around the designed mode-transition speed to prevent chattering between the operating modes. The absolute rotor speed $|\omega_r|$ must be greater than ω_{T1} for a dc-to-ac mode transition. An ac-to-dc mode transition is initiated when $|\omega_r|$ is below ω_{T2}, with $\omega_{T1}>\omega_{T2}$. For cases where the braking torque is insufficient to cause reverse power flow in the stator even with the drive speed lower than ω_{T2}, a secondary transition speed ω_{T3} is selected, where $\omega_{T2}>\omega_{T3}$. As the rotor speed reaches ω_{T3} while decelerating, being in ac mode, a braking torque is commanded at the shaft with the speed controller disabled. The delay T_d introduced between enabling gate signals to the succeeding SCR bank and the concluding SCR bank depends on the turn-off time of the chosen SCRs.

A phase-sequence change-over relay is connected between the ac source and the SCR-based transfer switch to extend the DFM drive operation range to all four quadrants. The relay operates only during the dc-mode operation of the drive with a hysteresis band around zero speed. The ac-source phase

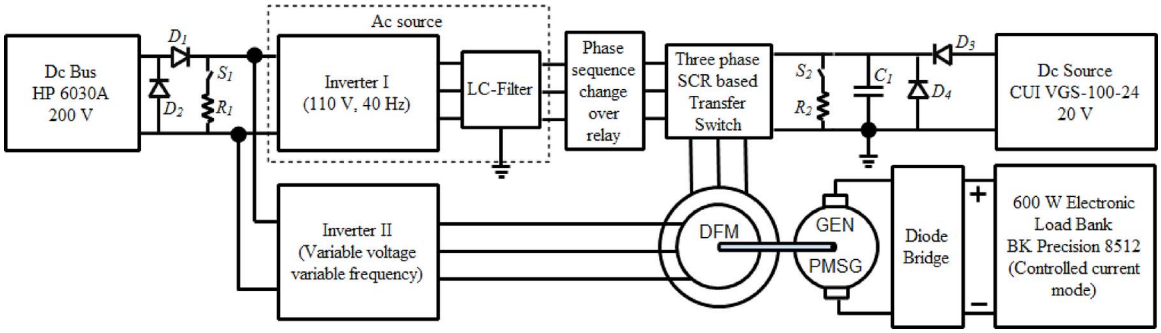

Fig. 10. Experimental setup used to demonstrate the proposed drive. In practice, the ac source created using the open-loop inverter and the LC filter will be replaced by a prime-mover-driven synchronous generator or an ac grid.

sequence is commanded to be ABC for rotor speed greater than ω_{T0} and ACB for drive speed less than $-\omega_{T0}$, where $\omega_{T0} < \omega_{T3}$. This prevents on-load operation of the relay. As an alternative, the relay can be replaced with two additional antiparallel SCRs cross-connecting the phases of the DFM with the ac source. This also increases operational reliability for applications that need frequent four-quadrant operation, replacing the mechanical operation of relay contact surfaces.

IV. Experimental Results

A 1-HP, 220-V/150-V, 60-Hz, and four-pole DFM has been used to illustrate the proposed switched-DFM drive. Two Texas Instruments High Voltage Motor Control and PFC Developer's Kits, named Inverter-I and Inverter-II and connected to a common dc bus, are used for the demonstration. Inverter-I is programmed to operate open-loop pulsewidth modulation, generating 110 V (phase peak) and 40 Hz (fundamental), as shown in Fig. 10. An output LC filter is used to filter the harmonics of Inverter-I and generate sinusoidal ac voltages emulating an ac source. The choice of ac-source voltage and frequency is selected such that the drive operates within the rated operating speed of the prototype DFM.

In practice, Inverter-I and the output LC filter will be replaced with an ac source generated using a prime-mover-driven synchronous generator or an ac grid. Inverter-II is programmed with the control algorithm developed for switched-DFM drive as described in [11]. The dc bus that feeds power to both the inverters is generated using a 200-V power supply. The two diodes D_1 and D_2 are used to prevent any reverse power flow to the power supply. The switch S_1 and the braking resistor $R_1(110\ \Omega)$ are used to dissipate power and limit the dc-bus voltage during braking operation of the drive. In practice, the dc bus will be created using a front-end converter interfacing the synchronous generator or the ac grid, as shown in Fig. 1.

The dc source is a separate 20-V power supply. Two diodes D_3 and D_4 and a capacitor C_1 (film-type, 16 uF) are added at the output of the dc source to emulate a rectified dc source. The switch S_2 and the resistor $R_2(10\ \Omega)$ dissipate power and maintain the dc-source voltage at the DFM terminal during the ac-to-dc source transition. The DFM is also mechanically coupled to a permanent-magnet synchronous generator (PMSG) that is connected to a dc electronic load bank through a diode bridge. The diode bridge helps in maintaining the polarity of

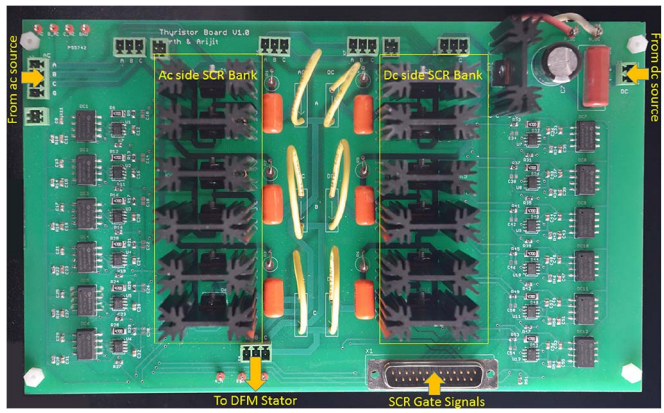

Fig. 11. Prototype SCR-based transfer switch used for the experimental demonstration.

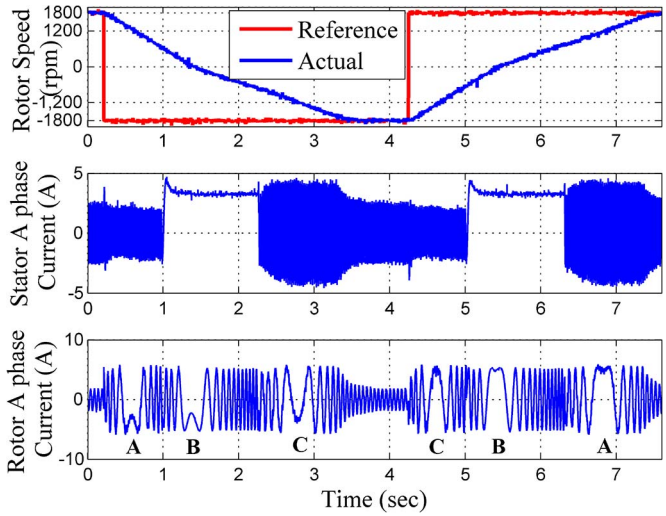

Fig. 12. Evaluation of the performance of the drive across the complete operating speed range. (Top) Speed response for a step command in reference speed; the different acceleration and deceleration rates at different speed ranges is as per the drive design. (Middle) Stator current that is either fixed-frequency (40 Hz) ac or dc. (Bottom) Controlled rotor current with operating frequency in the range of 0–24 Hz: (A)—drive speed is at positive ac-source synchronous speed; (B)—drive speed is at zero speed (equivalent to dc synchronous speed); (C)—drive speed is at negative ac-source synchronous speed.

the generated voltage connected to the load bank, irrespective of the direction of rotation of the PMSG. The electronic load bank is commanded to draw load current based on the operating speed of the DFM drive. This can emulate different types of

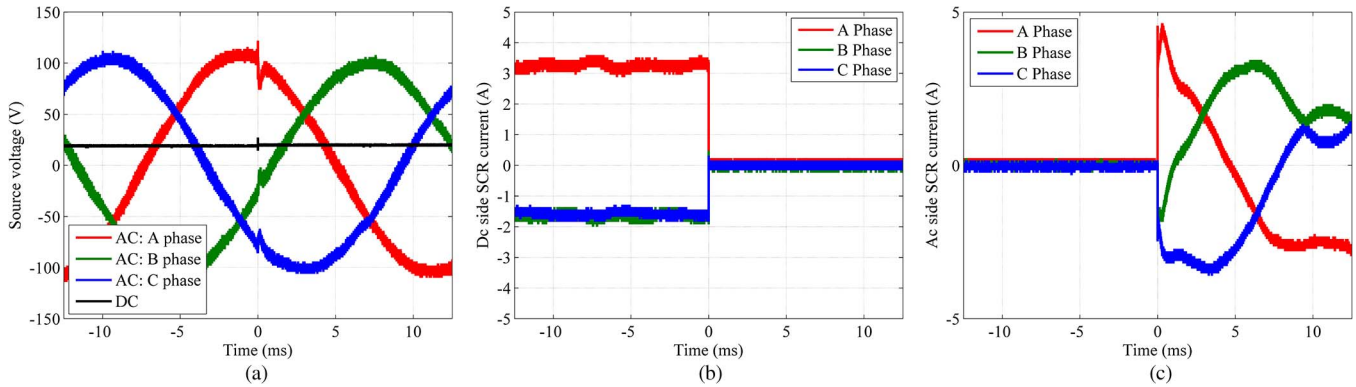

Fig. 13. Performance of the SCR-based transfer switch during dc-to-ac source transition. The source transition occurs at $t = 0$. (a) AC- and DC-source voltages during the transition. (b) DC-side SCR currents go to zero at the instant of transition. (c) AC-side SCRs pick up the DFM stator current seamlessly after the transition.

load profiles including the quadratic load torque curve that is typical for a ship propeller. The parameters of the DFM and the PMSG are shown in Table I.

The prototype SCR-based transfer switch built is shown in Fig. 11. Additionally, diodes are in series with each SCR to enable faster turn-off during mode transition. An RC snubber of 330 Ω and 6.8 nF is connected in parallel with the SCRs to limit the dv/dt stress. In practice, the window of $\pm 30^\circ$ for natural commutation of outgoing SCRs, as shown in Fig. 6, might need to be reduced taking into account the dead time of the SCRs. For example, considering a turn-off time of 250 μs for the chosen SCR will result in the allowable window to be $\pm 24^\circ$ (for a 60-Hz ac source) for safe commutation of the outgoing SCRs. Proper design with the fast-recovery high-power diodes can enable reducing this required dead time for high-power applications.

The experiments performed on the complete drive evaluate the SCR switch as well as the DFM operation under different loading conditions, explained in the following sections. The ac-source synchronous speed for the drive is 1200 r/min. The designed dc-to-ac source transition speed, i.e., ω_{T1}, and the ac-to-dc source transition speed, i.e., ω_{T2}, are 720 and 684 r/min, respectively. The ac-to-dc secondary transition speed is chosen as 648 r/min. Finally, the chosen phase change-over speed, i.e., ω_{T0}, is 30 r/min.

A. Performance of the Three-Phase SCR-Based Transfer Switch

With the DFM initially operating at 1800 r/min, two successive steps of -1800 and 1800 r/min is commanded to the reference speed as shown in Fig. 12. This evaluates the speed performance of the drive across the complete speed range under no load. The phase-sequence change-over relay and the SCR-based transfer switch seamlessly transfers the stator between the different operating regimes. The stator current A-phase current is either dc or 40 Hz depending on the operating speed, whereas the rotor A-phase current is appropriately controlled using Inverter-II.

Fig. 13 shows the performance of the SCR-based transfer switch during the instant of dc-to-ac mode transition. The mode transition occurs at $t = 0$ when the ac source A-phase voltage is greater than dc-source voltage and the ac source B and C phase voltages are negative, as shown in Fig. 13(a). Initially, the dc-side SCRs $T^A_{\mathrm{dc},F}$, $T^B_{\mathrm{dc},R}$, and $T^C_{\mathrm{dc},R}$ conduct [see Fig. 13(b)]. After the transition, the ac-side SCRs start conducting, as shown in Fig. 13(c), without any discontinuity in the DFM stator current.

Similarly, Fig. 14 shows the performance of the transfer switch during the ac-to-dc source transition. At the instant of the transition $(t = 0)$, the rotor power converter ensures that the phase currents are of opposite polarity to that of the ac-source phase voltages for simultaneous natural commutation of all the three phases as can be seen in Fig. 14(a) and (b). The DFM stator current transitions seamlessly from the ac source to the dc source as shown in Fig. 14(c). After the DFM stator is transitioned to the dc source, the stator A-phase current is initially negative. During this instant, the switch S_2 is turned on, and power is dissipated in the resistance R_2, thereby maintaining the dc voltage across the capacitor C_1.

B. Performance of the DFM Drive With the SCR-Based Transfer Switch

The performance of the proposed switched-DFM drive under different operating conditions is evaluated next. The electronic load bank is programmed to draw current proportional to the square of the rotor speed. This emulates a quadratic load-torque curve similar to a typical ship propulsion load. The step response of the DFM drive for the full-speed-range four-quadrant operation is shown in Fig. 15(a). In this case, the drive-torque capability for the complete speed range, along with the load torque, is shown in Fig. 15(b). The drive torque and the speed of the DFM are seamlessly controlled across the complete speed range. In a ship, this kind of requirement can arise during crash-back situations. The braking torque in the ac mode is commanded such that the drive can operate at unity power factor as required for the natural commutation of the ac-side SCRs. The active power shared between the stator and the rotor of the DFM is shown in Fig. 15(c) for the positive drive torque across the complete speed range. As designed, the rotor power electronics handles only a third of the total active power that is fed to the DFM for the complete speed range. The sharing of power for the negative-drive-torque case is a mirror image of the profile shown in Fig. 15(c) along the y-axis.

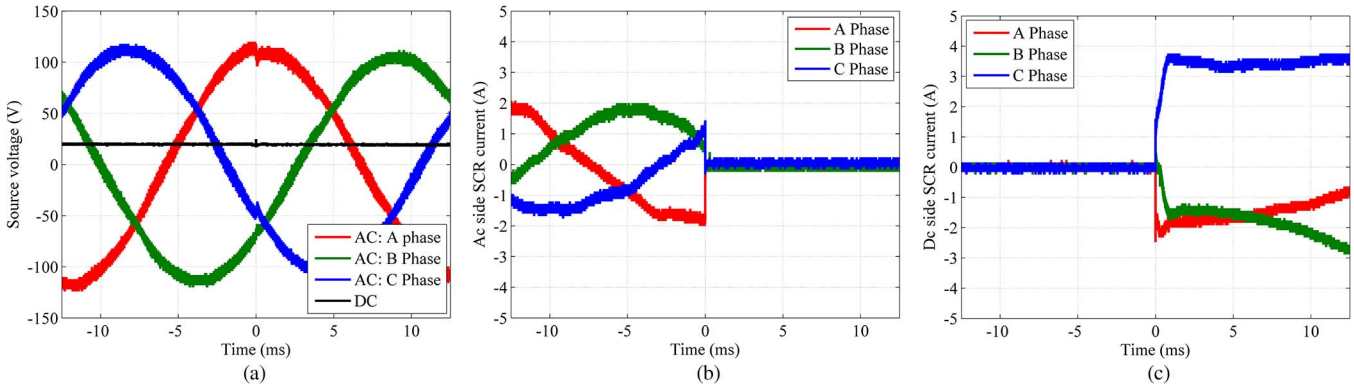

Fig. 14. Performance of the SCR-based transfer switch during ac-to-dc source transition. The source transition occurs at $t = 0$. (a) AC- and DC-source voltages during the transition. (b) AC-side SCR currents go to zero at the instant of transition. (c) DC-side SCRs pick up the DFM stator current seamlessly after the transition.

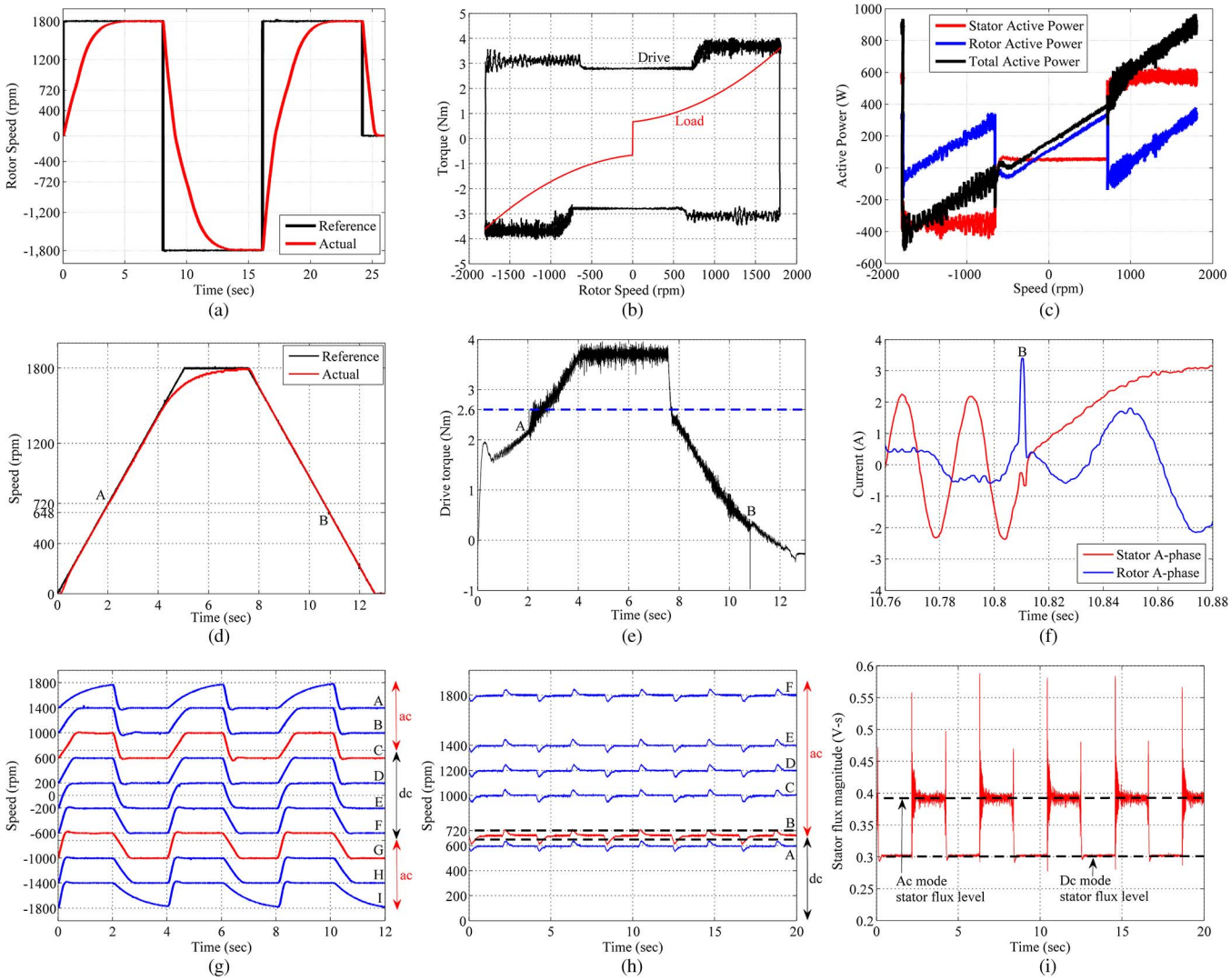

Fig. 15. Performance of the proposed switched-DFM drive subjected to different operating conditions. (a) Speed response of the DFM for step command in the reference speed. (b) Four-quadrant drive-torque speed capability along with total load torque (sum of the programmed PMSG torque, the static frictional torque, and the rotational frictional torque). (c) Sharing of active power of the DFM during the positive-torque demand for all speeds. Rotor power is a third of the total power being fed to the DFM. (d) Speed response of the DFM for a ramp command at the reference speed. (e) Corresponding drive torque during the ramp command at the reference speed. (f) Controlled rotor current of the DFM to ensure proper ac-side SCR commutation during ac-to-dc source transition. (g) Speed response of the DFM for alternating reference speed command with a step size of 400 r/min. (h) Speed response of the DFM under load torque disturbance, ranging between no-load and 70% of the rated load. (i) Stator-flux oscillation between the dc-mode and the ac-mode levels caused by a mode transition during the load disturbance corresponding to the profile B in (h).

To evaluate the performance of the drive under the reduced-drive-torque requirement at the transition speeds, a ramp is commanded in the reference speed with a slope of 360 r/min/s. The speed response of the drive is shown in Fig. 15(d), along with the commanded drive torque in Fig. 15(e). During acceleration, the demanded drive torque at the dc-to-ac transition instant (marked as A) is 2.2 Nm, whereas the "low drive torque" limit for the prototype drive calculated using (8) is 2.6 Nm. During deceleration at instant B, the rotor speed goes below the chosen secondary transition speed of 648 r/min. The commanded drive torque required, even at this rotor speed, is still positive such that the ramp down in speed can be maintained. In this case, the requirement of reverse power flow for the natural commutation of the ac-side SCRs cannot be met. As explained, a short pulse of a negative torque, as can be seen at B in Fig. 15(e), ensures the correct condition for the natural commutation of the outgoing ac-side SCRs and a source transition to dc source is achieved. The corresponding A-phase stator and rotor currents of the DFM are shown during this ac-to-dc transition. The speed response of the DFM is unperturbed, and the ramp speed response is achieved without distortion.

Next, the drive is subjected to an alternating reference speed across the complete speed range as shown in Fig. 15(g). The reference speed oscillates with a step size of 400 r/min at 0.5 Hz across the entire speed range. The speed response profiles A and B are completely in ac mode with positive ac-source frequency. The profiles D, E, and F are completely in dc mode, and the profiles H and I are again in ac mode with stator ac-source phase sequence reversed. The speed profiles C and G correspond to the case when the DFM drive partially operates in the dc and ac modes across the designed transition speed. As can be seen, the mode transitions are seamless even with an alternating reference speed. The settling time of the speed response increases with the operating speed because of the increase in the load torque (as programmed using the electronic load bank).

Finally, the drive is subjected to a load disturbance of zero to 70% of the rated load at different operating speeds, as shown in Fig. 15(h). The speed response profile A remains completely in dc mode for the load disturbance, and the profiles C, D, E, and F are completely in ac mode. For profile B, the reference speed is set at 684 r/min, which is midway between the dc-to-ac source transition speed (720 r/min) and secondary ac-to-dc transition speed (648 r/min). As the load goes to zero, the rotor speed overshoots beyond 720 r/min, leading to a dc-to-ac source transition. Eventually, the speed settles to 648 r/min operating in the ac mode. At the next instant when the drive is subjected to the 70% rated load, the rotor speed falls below the secondary transition speed of 648 r/min, leading to an ac-to-dc source transition. This can be seen in the stator-flux magnitude, shown in Fig. 15(i). The stator-flux magnitude oscillates between the designed dc-mode level and the ac-mode level, as set by the ac source. The drive performance is stable and equivalent without any notable differences under all operating regimes.

The phase-plane analysis used to ascertain the proper switching instant during an ac-to-dc source transition is experimentally validated, as shown in Fig. 16. Different initial conditions of δ, depending on the switching instant, lead to the different trajectories of the stator-flux magnitude from the ac-mode level to the dc-mode level. As expected, for Case A, the stator flux collapses during the ac-to-dc transition, leading to uncontrolled shaft torque.

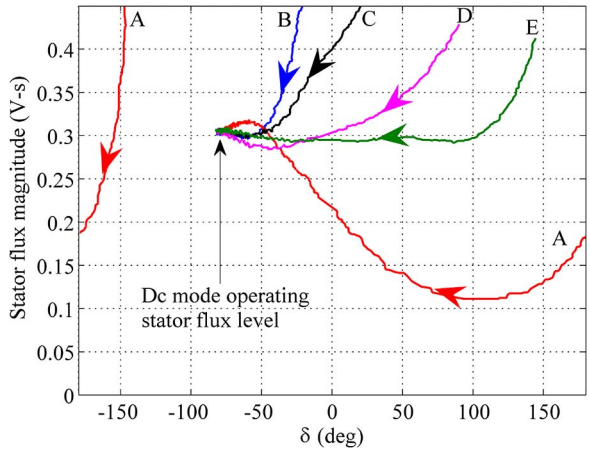

Fig. 16. Experimental validation of the stator-flux trajectory during ac-to-dc transition, based on the initial condition of δ that depends on the switching instant.

V. Conclusion

This paper has presented and demonstrated an SCR-based STS that can change stator supply between an ac and a dc source on-the-fly for a switched-DFM drive. Rotor-current control not only allows bumpless transition between modes but also enables reduction of SCR commutation circuits by controlling the phase angle between the stator voltage and the stator current during the transitions. Using SCRs to construct the transfer switch, while allowing instantaneous transition without shorting the sources or impairing the load currents, enables significant reduction of controlled power electronics and associated passive-auxiliary components. With no additional circuit required for the commutation of the SCRs and reduced rotor converter size, the proposed transfer-switch-based drive architechture is a cost-effective solution suitable for high-power applications. The proposed transfer switch opens up a mechanism for operation of the switched-DFM drive that can be adjusted based on the specific drive design and transient performance requirement. With the availability of high-power SCRs with large short-time current ratings, a hybrid transfer switch with parallel mechanical relays can be devised to reduce losses (conduction) in the transfer switch to an even greater extent.

References

[1] S. Kouro, J. Rodriguez, B. Wu, S. Bernet, and M. Perez, "Powering the future of industry: High-power adjustable speed drive topologies," *IEEE Ind. Appl. Mag.*, vol. 18, no. 4, pp. 26–39, Jul. 2012.

[2] C. Lewis, "The advanced induction motor," in *Proc. IEEE Power Eng. Soc. Summer Meet.*, Jul. 2002, vol. 1, pp. 250–253.

[3] A. Tessarolo, G. Zocco, and C. Tonello, "Design and testing of a 45-MW 100-Hz quadruple-star synchronous motor for a liquefied natural gas turbo-compressor drive," *IEEE Trans. Ind. Appl.*, vol. 47, no. 3, pp. 1210–1219, May/Jun. 2011.

[4] R. Lateb *et al.*, "Performances comparison of induction motors and surface mounted PM motor for POD marine propulsion," in *Conf. Rec. 40th IEEE IAS Annu. Meeting*, Oct. 2005, vol. 2, pp. 1342–1349.

[5] E. Muljadi, M. Singh, and V. Gevorgian, "Doubly fed induction generator in an offshore wind power plant operated at rated V/Hz," *IEEE Trans. Ind. Appl.*, vol. 49, no. 5, pp. 2197–2205, Sep./Oct. 2013.

[6] A. Hassannia and A. Darabi, "Design and performance analysis of superconducting rim-driven synchronous motors for marine propulsion," *IEEE Trans. Appl. Supercond.*, vol. 24, no. 1, pp. 40–46, Feb. 2014.
[7] J. Rodriguez *et al.*, "Design and evaluation criteria for high power drives," in *Conf. Rec. IEEE IAS Annu. Meeting*, Oct. 2008, pp. 1–9.
[8] B. Wu, *High-Power Converters and AC Drives*. Piscataway, NJ, USA: Wiley, 2006.
[9] S. Muller, M. Deicke, and R. De Doncker, "Doubly fed induction generator systems for wind turbines," *IEEE Ind. Appl. Mag.*, vol. 8, no. 3, pp. 26–33, May/Jun. 2002.
[10] A. Banerjee, M. Tomovich, S. Leeb, and J. Kirtley, "Power converter sizing for a switched doubly fed machine propulsion drive," *IEEE Trans. Ind. Appl.*, vol. 51, no. 1, pp. 248–258, Jan./Feb. 2015.
[11] A. Banerjee, M. S. Tomovich, S. B. Leeb, and J. L. Kirtley, "Control architecture for a switched doubly fed machine propulsion drive," *IEEE Trans. Ind. Appl.*, vol. 51, no. 2, pp. 1538–1550, Mar./Apr. 2015.
[12] Y.-H. Chung, "Medium voltage hybrid transfer switch," in *Proc. IEEE Power Eng. Soc. Winter Meet.*, 2002, vol. 2, pp. 1158–1163.
[13] D. Ransom, "Choosing the correct transfer switch," *IEEE Trans. Ind. Appl.*, vol. 49, no. 6, pp. 2820–2824, Nov./Dec. 2013.
[14] L. Morel, H. Godfroid, A. Mirzaian, and J.-M. Kauffmann, "Double-fed induction machine: Converter optimisation and field oriented control without position sensor," *Proc. Inst. Elect. Eng.—Elect. Power Appl.*, vol. 145, no. 4, pp. 360–368, Jul. 1998.
[15] X. Yuan, J. Chai, and Y. Li, "A converter-based starting method and speed control of doubly fed induction machine with centrifugal loads," *IEEE Trans. Ind. Appl.*, vol. 47, no. 3, pp. 1409–1418, May/Jun. 2011.
[16] S. Bernet, "Recent developments of high power converters for industry and traction applications," *IEEE Trans. Power Electron.*, vol. 15, no. 6, pp. 1102–1117, Nov. 2000.
[17] J. Farber, D. C. Griffith, and A. Pflieger, "Static inverter standby ac power for generating station controls," *IEEE Trans. Power App. Syst.*, vol. PAS-87, no. 5, pp. 1270–1274, May 1968.
[18] T. Wolpert, "Uninterruptible power supply for critical ac loads—A new approach," *IEEE Trans. Ind. Appl.*, vol. IA-10, no. 5, pp. 627–634, Sep./Oct. 1974.
[19] J. Schwartzenberg and R. De Doncker, "15 kV medium voltage static transfer switch," in *Conf. Rec. IEEE IAS Annu. Meeting*, Oct. 1995, vol. 3, pp. 2515–2520.
[20] H. Mokhtari, S. Dewan, and M. Travani, "Performance evaluation of thyristor based static transfer switch," *IEEE Trans. Power Del.*, vol. 15, no. 3, pp. 960–966, Jul. 2000.
[21] B. Tian *et al.*, "400 V/1000 kVa hybrid automatic transfer switch," *IEEE Trans. Ind. Electron.*, vol. 60, no. 12, pp. 5422–5435, Dec. 2013.
[22] *IEEE Recommended Practice for Emergency and Standby Power Systems for Industrial and Commercial Applications*, IEEE Std 446-1995 (The Orange Book), Jul. 1996, pp. 1–320
[23] H. Mokhtari and M. Iravani, "Effect of source phase difference on static transfer switch performance," *IEEE Trans. Power Del.*, vol. 22, no. 2, pp. 1125–1131, Apr. 2007.

Arijit Banerjee (S'12) received the B.E. degree in electrical engineering from Bengal Engineering and Science University, Howrah, India, in 2005 and the M.Tech. degree in electrical engineering from the Indian Institute of Technology Kharagpur, Kharagpur, India, in 2007. He is currently working toward the Ph.D. degree at the Massachusetts Institute of Technology, Cambridge, MA, USA.

During 2006–2007, he was a Visiting Student with the Institute for Power Electronics and Control of Drives, Technische Universität Darmstadt, Darmstadt, Germany, under a German Academic Exchange Service (DAAD) Fellowship. From 2007 to 2011, he was with the Power Conversion Systems Group, General Electric Global Research Centre, Bangalore, India, where he was working on monitoring and diagnostics of electromechanical systems using electrical signatures. In 2011, he joined the Laboratory for Electromagnetic and Electronic Systems, Massachusetts Institute of Technology. He is the holder of ten issued patents and several patent applications. His research interests include analysis, design, control, and diagnostics of electromechanical systems.

Arthur H. Chang (S'09) received the B.S. and M.S. degrees in electrical engineering from the California Institute of Technology, Pasadena, CA, USA, in 2009 and 2010, respectively. He is currently working toward the Ph.D. degree in electrical engineering and computer science at the Massachusetts Institute of Technology (MIT), Cambridge, MA, USA, where he is affiliated with the Laboratory of Electromagnetic and Electronic Systems.

Mr. Chang was a recipient of the National Defense Science and Engineering Graduate Fellowship (2009–2012), the Analog Devices Outstanding Student Designer Award (2010), and the Applied Power Electronics Conference and Exhibition Outstanding Technical Presentation Awards (2013 and 2014). He was also the grand prize winner of the MIT Clean Energy Prize (2014) and a recipient of the Tau Beta Pi (Williams No. 30) Fellowship (2009) and the Caltech Upper Class Carnation Merit Scholarship (2008).

Kawin North Surakitbovorn was born in Thailand in 1990. He received the B.S. degree in physics and electrical engineering from the Massachusetts Institute of Technology, Cambridge, MA, USA, in 2014. He is currently working toward the Ph.D. degree in electrical engineering at Stanford University, Stanford, CA, USA.

He initially worked on fabrication of graphene devices and later on power electronics and motor control. His interest is in power electronics, particularly in applications of high-frequency power converters.

Steven B. Leeb (F'07) received the Ph.D. degree from the Massachusetts Institute of Technology (MIT), Cambridge, MA, USA, in 1993.

He has served as a Commissioned Officer in the U.S. Air Force Reserve Command and has been a member of the MIT faculty in the Department of Electrical Engineering and Computer Science since 1993. He also holds a joint appointment with MIT's Department of Mechanical Engineering. He currently serves as a MacVicar Fellow and Professor of electrical engineering and computer science with the Laboratory for Electromagnetic and Electronic Systems. He is the author or coauthor of over 80 publications and 13 U.S. patents in the fields of electromechanics and power electronics. In his capacity as a Professor at MIT, he is concerned with the design, development, and maintenance processes for all kinds of machinery with electrical actuators, sensors, or power electronic drives.

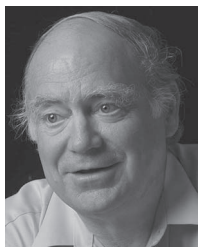

James L. Kirtley, Jr. (F'90–LF'91) received the Ph.D. degree from the Massachusetts Institute of Technology (MIT), Cambridge, MA, USA, in 1971.

He is a Professor of electrical engineering with MIT. He was with General Electric, Large Steam Turbine Generator Department, as an Electrical Engineer and with SatCon Technology Corporation as Vice President and General Manager of the Tech Center and as Chief Scientist and Director. He was Gastdozent at the Swiss Federal Institute of Technology. He is a specialist in electric machinery and electric power systems.

Dr. Kirtley served as Editor-in-Chief of the IEEE TRANSACTIONS ON ENERGY CONVERSION from 1998 to 2006 and continues to serve as Editor for that journal and as a member of the Editorial Board of *Electric Power Components and Systems*. He was awarded the IEEE Third Millennium Medal in 2000 and the Nikola Tesla Prize in 2002. He was elected to the United States National Academy of Engineering in 2007. He is a Registered Professional Engineer in Massachusetts.